Compact MR Rotary Brake for Prosthetic Applications

Gunnar Sveinn Rúnarsson

Faculty of Mechanical Engineering
University of Iceland
2017

Compact MR Rotary Brake for Prosthetic Applications

Gunnar Sveinn Rúnarsson

30 ECTS thesis submitted in partial fulfillment of a
Magister Scientiarum degree in Mechanical Engineering

MS Committee
Fjóla Jónsdóttir
Heimir Tryggvason

Master's Examiner
Sigurður Brynjólfsson

Faculty of Mechanical Engineering
School of Engineering and Natural Sciences
University of Iceland
Reykjavik, May 2017

Compact MR Rotary Brake for Prosthetic Applications
Compact MR Rotary Brake in Prosthetics
30 ECTS thesis submitted in partial fulfillment of a *Magister Scientiarum* degree in Mechanical Engineering

Faculty of Industrial Engineering, Mechanical Engineering and Computer Science
School of Engineering and Natural Sciences
University of Iceland
VRII, Hjarðarhagi 2-6
107, Reykjavik
Iceland

Telephone: 525 4000

Bibliographic information:
Gunnar Sveinn Rúnarsson 2017, Compact MR Rotary Brake for Prosthetic Applications, Master's thesis, Faculty of Industrial Engineering, Mechanical Engineering and Computer Science, University of Iceland.

Printing: Háskólaprent
Reykjavik, Iceland, May 2017

Abstract

Controllable stiffness can greatly improve the usefulness of a prosthetic foot and its users comfort. In this thesis the feasibility of using a magnetorheological rotary brake in conjunction with carbon fiber blades to provide variable stiffness in a prosthetic foot is investigated. For the brake to be effective in a prosthesis it needs to be compact. A known reference design, currently used in a prosthetic knee, is scaled down and a finite element analysis applied to investigate the effect chosen parameters have on the torque output. The size is investigated with regard to the radius of the brake because of limited space as well as weight restrictions. The minimum torque output needs to be high enough to provide a range for the stiffness to be considered variable and have an effect on the prosthesis behavior. The results show that a magnetorheological brake retains enough braking torque after being scaled down to be considered an option in a foot prosthesis.

Útdráttur

Stýranleg stífni getur aukið notagildi gervifótar auk þess að veita notanda meiri stjórn og þægindi. Í þessari ritgerð er skoðað hvort físilegt er að nota rafsegulvökva bremsu í bland við blöð úr kolefnistrefjum til þess að gera stífni gervifóta breytilega. Til þess að hægt sé að nýta bremsuna í gervifót þarf hún að vera lítil og létt. Þekkt hönnun er notuð til viðmiðunar og sköluð niður. Sérstakur hugbúnaður er notaður við líkanagerð til þess að skoða hvaða áhrif valdar breytur hafa á bremsuvægi. Stærð bremsunar er skoðuð með tilliti til radíusar þar sem takmarknir eru á svæðinu í kringum lið og þyngd. Lágmarks bremsuvægi þarf að vera nægilega mikið til þess að stífni geti talist breytileg og til þess að hafa áhrif á eiginleika gervifótar. Niðurstöður sýna að rafsegulvökva bremsan skilar nægilega miklu bremsuvægi eftri að vera minnkuð til þess að geta talist ákjósanlegur kostur.

Table of Contents

List of Figures

List of Tables

Acknowledgements

I would like to thank my advisors Dr. Fjóla Jónsdóttir and Phd student Heimir Tryggvason for their help and support. I also want to thank Össur hf. for the information provided to perform the study. Last but not least I would like to thank my parents for their support and my mother for always being willing to proofread my thesis.

1 Introduction

When a new prosthesis is designed the goal is always to have it to resemble the lost limbs functions as closely as possible. This poses a great challenge as the human body is very flexible and adaptive. Research show that for low level activity, such as walking at slow to normal speeds, the behavior of an ankle can be imitated by a passive spring and damper system [1]. For this, somewhat limited, everyday use there is a variety of constant stiffness prosthetic feet commercially available. When the activity level increases however, the complexity of the function and muscular activity in the physiological ankle increases as well. This complexity provides a challenge for designers of prosthetic devices who need to find a way to make them adaptable to change in activity level, terrain or other situations.

This can be achieved to some extent by making the stiffness of the joints controllable for these different actions and the different forces that act on the prosthetic device. Magnetorheological (MR) rotary brake has been successfully implemented in a prosthetic knee joint, the Rheo Knee® by Össur, providing control of the stiffness in the joint [2]. The aim of this research is to investigate the adaptation of this magnetorheological brake to a joint in a prosthetic foot, to provide active control of its stiffness in conjunction with carbon fiber blades. This requires the brake to be scaled down due to size and weight limitations in the prosthetic foot. The feasibility of this approach will be weighed on how much torque output the brake retains in its compact version. Different parameters will be investigated in terms of the effect they have on the size and torque output of the brake and compared to the original version. This is an analytical research where a finial element model is used to simulate the MR rotary brake.

Prosthetic feet with passive stiffness are still the most common design, with a wide range of types for different activities. Implementing controllable stiffness via MR technology has been studied on different occasions. The use of MR dampeners has been studied [3] and patented [4] but due to weight and loss of energy in the dampener, the design has not been successful. The use of magnetorheological elastomers (MRE) to achieve controllable stiffness has been investigated [5], but not used for production. Powered prosthetic feet are commercially available though expensive [6, 7]. With constant ongoing development this might change in the future.

Controllable stiffness can be achieved through different methods in a prosthetic foot, but for it to become commercially successful there are many things to consider, such as weight, cost and power consumption. This thesis however focuses on finding out if an MR rotary brake is a viable option for a prosthetic foot. Can it be scaled down and still maintain enough torque to provide a range of stiffness for future users?

The reminder of the thesis is organized as follows.

In chapter 2 MR technology is described. The fluid characteristics and composition, the most common commercial uses, the MR rotary brake and its torque output.

Chapter 3 describes the design of the prosthetic foot as well as the design parameters.

In chapter 4 the finite element model is discussed as well as the B-H curves used to define the material properties in the model.

Chapter 5 contains a parameter study of chosen parameters and how they affect the braking torque of the MR rotary brake.

Chapter 6 concludes the thesis with proposals for future work.

2 MR Technology

MR technology is based on materials with variating rheological properties. The variation is triggered by magnetic fields and controlled via solid-state electronics and modern control algorithms. These materials are a part of a group of materials that are commonly referred to as smart materials [8].

MR fluids were initially discovered and developed by inventor Jacob Rabinow at the US National Bureau of Standards in the late 1940s [9]. Commercial success on the other hand did not come until the 1990s when a number of MR fluid-based systems were released, such as a fluid brake used in the exercise industry and a controllable damper used in truck seat suspension [10].

MR Fluids

MR fluids are composed of high concentration of magnetizable particles in an non-magnetic medium where the size, concentration and material selection of the particles varies depending on what is required of the fluid. Iron particles are the most common due to their high saturation magnetization. Larger particles result in a more stable, highly magnetizable fluid and reversible particle aggregation [11].

The carrier fluid is chosen based on rheological and tribological properties as well as temperature stability. Most common carrier fluids are petroleum based oils, silicone, mineral oils, polyesters, polyethers, water and synthetic hydrocarbon oils. Other fluids may be added for additional lubricating properties or to inhibit sedimentation and agglomeration [11].

MR fluids magnetorheological response occurs when particles suspended in the fluid polarize due to the application of an external magnetic field. The induced dipoles form columnar structures that are parallel to the applied field and restrict the motion of the fluid, thereby increasing the viscous characteristics of the suspension. This can be observed in Figure 2-1 b). The mechanical energy needed to yield the microstructure increases as the magnetic field increases resulting in a field dependent yield stress. In the absence of an applied field, MR fluids exhibit Newtonian-like behavior [12] where the particles are randomly scattered in the fluid as demonstrated in Figure 2-1 a).

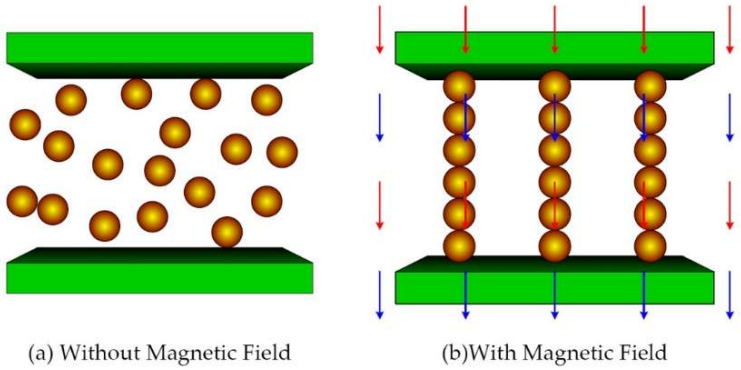

Figure 2-1. MR fluid a) without magnetic field and b) with magnetic field.

The MR fluid used in the reference design is patented under US patent specification 7,101,487 [13] and was developed with prosthetic applications in mind [2]. The carrier fluid has a shear-rate-independent viscosity of 0.3 Pa s which increases sedimentation stability [2]. The study is based on pre-defined fluid properties of a PFPE-based MR fluid [14]. It has a solid concentration of 0.28 by volume, using carbonyl iron particles with an average diameter of 2.5 µm. The Bingham model is used to characterize the constitutive behavior of the fluid [15] and is discussed later in this chapter.

Applications

As has been discussed, MR fluids can vary in physical properties depending on utilization. Devices relying on MR technology are used in a range of different fields and are commonly divided into three categories dependent on the flow mode they rely on; valve mode, shear mode and squeeze mode [16].

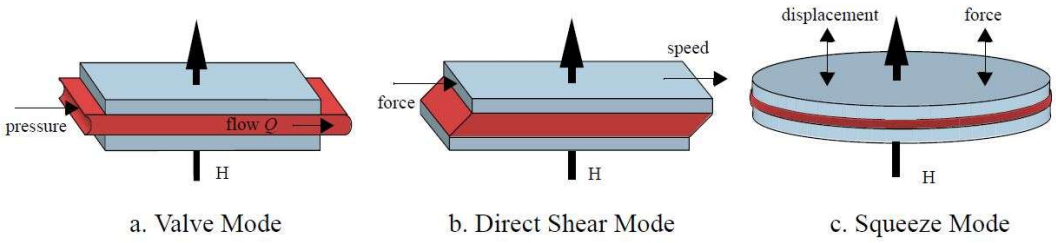

Figure 2-2. MR fluid used in a) valve mode, b) shear mode and c) squeeze mode. H is the magnetic field strength [11].

Figure 2-2 shows the different types of modes in which MR fluid is used. A device is said to operate in valve mode when the MR fluid is used to impede the flow of MR fluid from one reservoir to another. This mode is commonly used in MR dampers, zero-valves, shock absorbers and actuators, and is the most widely used of the three modes [11, 17]. A device using squeeze mode has a thin film of MR fluid sandwiched between paramagnetic pole surfaces [17]. This mode has been used for small amplitude vibration and impact dampers [18]. A device using shear mode has a thin layer of MR fluid sandwiched between two paramagnetic moving surfaces [17]. This mode has been used for clutches, brakes, chucking and locking devices, dampers and structural components [11]. An advantage of MR fluids is

the low power needed to control the fluid and can therefore be used with low voltage sources such as a lithium ion battery.

The MR rotary brake

MR technology has been utilized effectively in the prosthetic industry in recent years for prosthetic knee joints controlled via a microprocessor based on sensors in the leg. It was originally developed and designed by Herr et al [19] and Deffenbaug et al [20]. Prosthetic feet are most commonly manufactured using carbon fiber blades, and therefore there is no way to control the stiffness in the foot. Amputees partaking in diversions that require different stiffness from their day-to-day activities, like sports, often have special prosthetic feet suited for that purpose.

The objective of this thesis is to examine if it is possible to scale down a MR rotary brake used in the Rheo knee 3® [7], seen in Figure 2-3 (left), and use it effectively in a prosthetic foot similar to the one seen in Figure 2-3 (right), to implement controllable stiffness. To get a better understanding of the parameters and the formulation of the braking torque, a general overview of the MR rotary brake is needed.

Figure 2-3. Rheo Knee 3® (left) and Pro-Flex® foot (right) from Össur [7].

The MR rotary brake actuator is approximately axi-symmetric as can be seen in Figure 2-4, simplifying the finite element model as a 2D axi-symmetric instead of a 3D model. The brake utilizes the direct shear mode to produce braking torque when a magnetic field is applied.

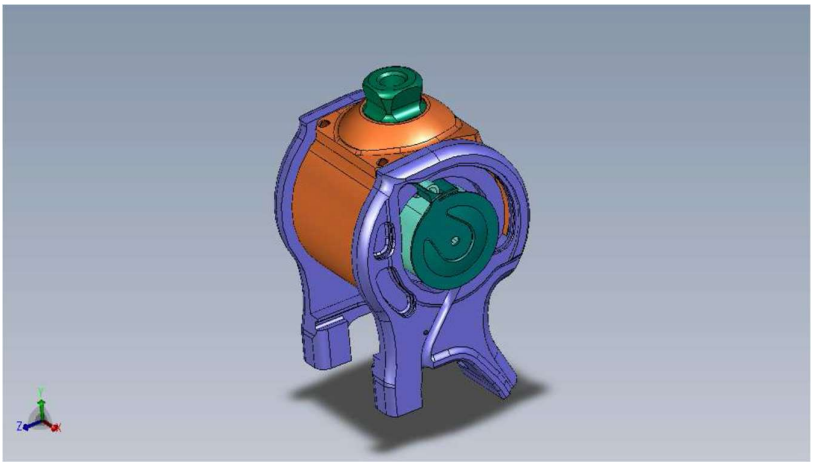

Figure 2-4. The MR rotary brake [7].

Figure 2-5 shows an overview of the layout of the original design of the MR rotary brake by Herr et al [19] and Deffenbaugh et al [20]. The magnetic field is produced by a copper coil wound around a cobalt-iron core and directed through the sides towards, and through the fluid chamber.

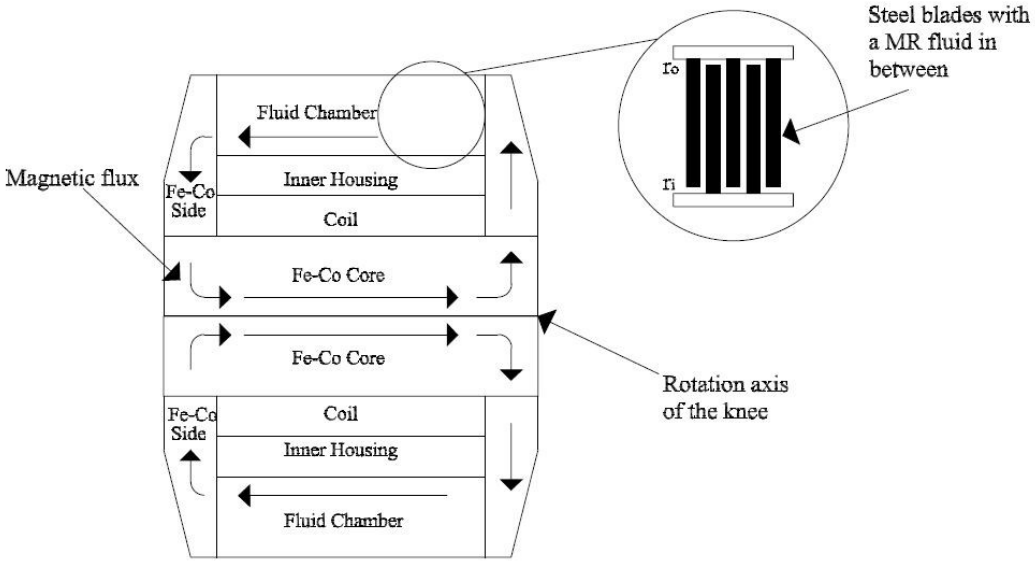

Figure 2-5. Overview of the layout of the magnetic circuit and the fluid chamber based on the original design of Herr et al (ref) [19] and Deffenbaugh et al [20].

The core and the sides are made from cobalt-iron alloy because of its high magnetic saturation value of 2.2 T [21].

The fluid chamber is fitted with tightly arranged steel blades connected alternately to the outer house (stator) and the inner house (rotor). The blades are relatively thick when compared to the micron sized gap between them, filled with MR fluid. This maximizes the area sheared by the fluid, hence maximizing the torque output when the blades shear the particle microstructures created when the magnetic field is applied. The rotor and stator are

separated by the MR fluid and in the reference design the stator is connected to the amputee's residual limb while the rotor is connected to the lower part of the leg [2]. In the prosthetic foot the rotary brake replaces a pivot joint, as is discussed further in chapter 3 and can be seen in Figure 3-1.

Prosthetics using MR rotary brakes can be used for a number of years with proper maintenance. The MR fluid degrades and needs to be changed after a period of time. Temperature has an effect on the viscosity of the MR fluid and the off-state rotary stiffness. This however has not introduced any problems[22].

Theoretical braking torque

To calculate the braking torque in the actuator the geometry of the braking torque is needed as well as the MR fluid parameters. The shear stress in the MR fluid is obtained via the linear Bingham model [23]. In this model the shear stress, τ, is given by

$$\tau = \tau_y(B) + \mu_{MR,P-Y}\dot{\gamma} \qquad (1)$$

where $\tau_y(B)$ is the yield stress, B is the average magnetic flux density (MFD) and $\mu_{MR,P-Y}$ is the post yield viscosity in the fluid.

When the fluid is sheared between two blades the shear strain rate is a function of the radius r, the gap between the blades, d, and the angular velocity, ω. This is expressed by

$$\dot{\gamma} = \frac{r\omega}{d} \qquad (2)$$

By combining equations 1 and 2 one obtains:

$$\tau(r) = \tau_y(B) + \mu_{MR,P-Y}\frac{r\omega}{d} \qquad (3)$$

The torque transmitted by a differential blade element is expressed by

$$dT = \tau(r)2\pi r^2 dr \qquad (4)$$

By combining equation 3 and 4 the torque transmitted by the shear in the gap is obtained:

$$T_{gap} = \frac{2}{3}\pi\tau_y(B)(r_o^3 - r_i^3) + \pi\mu_{MR,P-Y}\frac{\omega}{2d}(r_o^4 - r_i^4) \qquad (5)$$

where r_o is the outer radius of the blades,r_i is the inner radius of the blades and the post-yield viscosity of the MR fluid measured at 4 Pa s [2]. The shear operation occurs in each MR fluid gap, n, so multiplying equation (5) with n gives the braking torque of the MR brake when it is under the effect of a magnetic field:

$$T = \frac{2}{3}\pi\tau_y(B)n(r_o^3 - r_i^3) + n\pi\mu_{MR,P-Y}\frac{\omega}{2d}(r_o^4 - r_i^4) \qquad (6)$$

Off-state rotary stiffness determines how rigid the brake is while not under the effect of a magnetic field and is described by [2]:

$$T_{off-state} = n\pi\mu_{off}\frac{\omega}{2d}(r_o^4 - r_i^4) + T_b + T_o \qquad (7)$$

where μ_{off} is the off-state viscosity assumed to be 0.9 Pa s, T_b is friction in bearings measured to be 0.8 Nm and T_o is friction in oil seals measured to be 0.8 Nm. This is not a crucial factor in this thesis but needs to be taken into consideration since a high off-state rotary stiffness can cause problems and discomfort for the user.

The inner and outer radius of the MR rotary brake will be further discussed in chapter 3. For the theoretical braking torque to be calculated the shear stress must be known. In order to determine the yield stress the magnetic flux density (MFD) is required.

The MR fluid shear yield stress curve is represented by [22]

$$\tau_y = 29000 - 29000\cos\pi B \qquad (8)$$

where τ_y is the yield stress and B is the average MFD in the fluid. Figure 2-6 shows the shear-yield stress curve for the PFPE-based MR fluid. A finite element model is used to simulate the magnetic circuit in the brake to estimate the MFD in the fluid. Non-linear B-H curves represent the material properties [14].

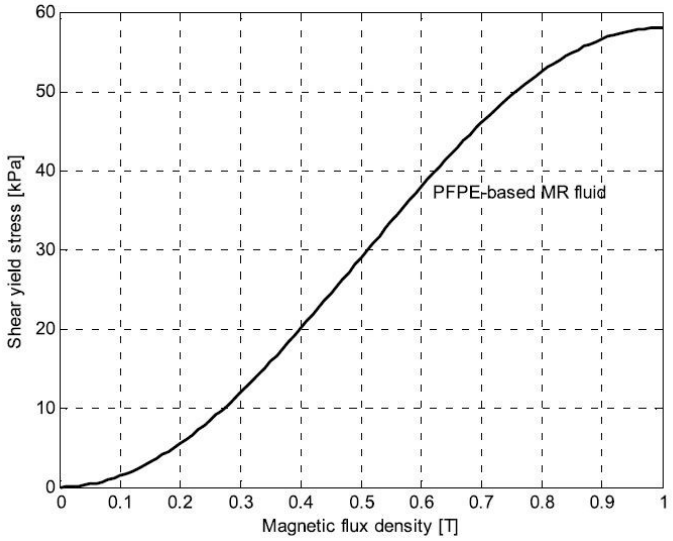

Figure 2-6. Shear yield stress vs. mangetic flux density [22].

3 Design overview

Research shows that for a 75 kg person, peak torque requirements for a normal walking speed is close to 120 Nm at maximum dorsiflexion [24]. Size and weight constrictions prevent the use of an MR rotary brake to provide all the required torque. In the proposed design a mix of passive and controlled stiffness is used where the passive stiffness comes from carbon fiber blades in the foot and the controlled stiffness from an MR rotary brake. Proposed design criteria for the minimum braking torque output is 20 Nm, as it is the stiffness difference between categories for carbon fiber blades in prosthetic feet.

Figure 3-1 shows the main components of the foot prosthesis. The bottom-, mid- and top blade provide the majority of the stiffness. The proposed placement of the brake is where the pivot joint is located and it needs to be compact since space is limited and added weight can cause problems and discomfort for the user. The reference design is the rotary brake from the Rheo Knee3® prosthetic knee and has been optimized for that purpose. It has a torque output of 61 Nm with outer radius, r_o, of 24 mm [22]. For the MR rotary brake to be compact enough for a prosthetic foot, the proposed design criteria for maximum outer radius is 20 mm.

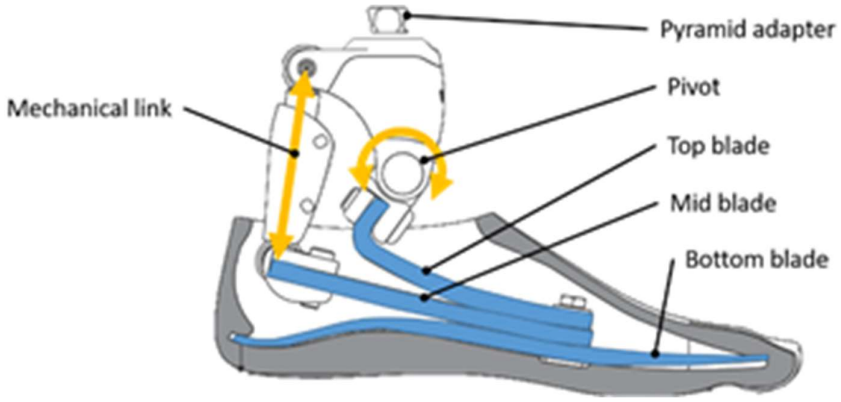

Figure 3-1. Overview of the foot prosthesis and its main components.

The width of the MR rotary brake is not changed significantly since it is not a limiting factor in the prosthetic foot. The width of the coil is unchanged from the reference design, 18.8 mm.

Figure 3-2 illustrates the design parameters used to calculate the size of the brake in terms of the radius, shown in equations 9 and 10.

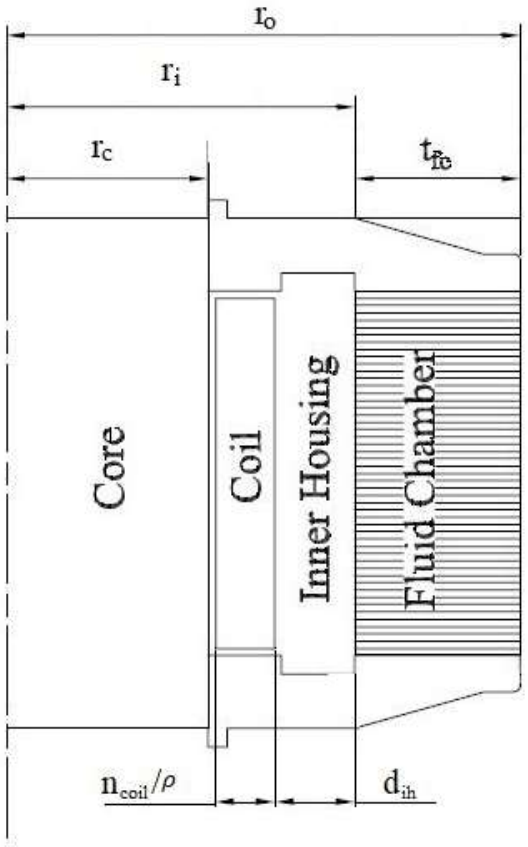

Figure 3-2. Overview of the MR rotary brake and its design parameters.

The inner radius of the fluid chamber, r_i, is determined by the radius of the core, the size of the coil and the size of the inner housing, as [2]

$$r_i = r_c + \frac{n_{coil}}{\rho} + d_{ih} \qquad (9)$$

where n_{coil} represents the number of windings in the coil, ρ is the coil's windings density and d_{ih} is the size of the inner house.

The outer radius of the fluid chamber, r_o, is determined by the inner radius and the thickness of the fluid chamber, t_{fc}:

$$r_o = r_i + t_{fc} \qquad (10)$$

The current amplitude in the coil is not a design parameter but is held at a constant value of 1.5 A. This is the maximum the voltage generator can generate. Current amplitude of 1.4 A is sufficient for the core to be at its saturation value [21], therefore it is not a limiting factor.

Table 3-1 lists the main design parameters of the MR rotary brake with a short description of each parameter and the reference design values. The parameters listed are used in the finite element model, but the main parameters investigated are the core radius, r_c, and the fluid chamber thickness, t_{fc}.

Table 3-1. List of design parameters.

Parameter	Description	Reference design
r_c	Radius of the core.	10.7 mm
n_{coil}	Number of windings in the coil.	310
t_{s1}	Initial thickness of the sides (at the core).	5.5 mm
t_{s2}	Final thickness of the sides (at the fluid chamber).	3.5 mm
t_s	Start of side thickness reduction (distance from the core).	14.0 mm
t_{fc}	Thickness of the fluid chamber.	6.5 mm
d	Distance between blades in the fluid chamber.	35 μm
n	Number of blades in the fluid chamber.	71
t_h	Thickness of inner house seat (side cut out).	0.60 mm

Together, equations 9 and 10 include all the design parameters affecting the radius of the MR rotary brake, width not being a concern for this research. Equation 6 shows that changing any of these parameters will affect the braking torque. To inspect the feasibility of a compact MR rotary brake in a prosthetic foot a parametric study is used. The calculations require a finite element model to simulate the magnetic circuit in the brake, which is discussed in the following chapter.

4 Finite element model

As was discussed in chapter 2 an important parameter for accurate calculation of the braking torque is the MFD in the MR fluid. This requires an accurate model of the magnetic circuit. A finite element model used in former researches [5, 21, 22, 25] exists. Its purpose has been to evaluate the magnetic flux density in the Rheo Knee's magnetic circuit.

The existing model was utilized for this research but adaptations were made since the former model was restricted concerning the size of the circuit. A finite element analysis gives a more accurate estimation of magnetic flux density in the fluid when compared to an analytical estimation.

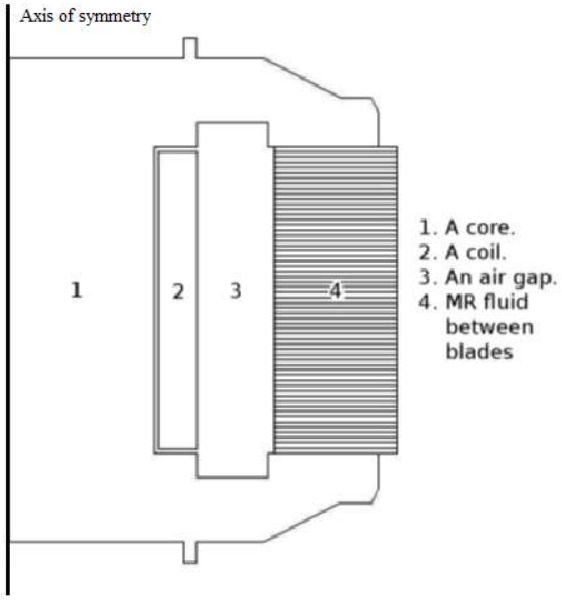

Figure 4-1. Schematic of a finite element model of the MR rotary brake [2].

Figure 4-1 shows the material configuration of the finite element model. Material 1 is the magnetic cobalt-iron alloy that is magnified by the coil and transfers the magnetic field through the sides to the fluid chamber. Material 2 is the copper coil that generates the magnetic field. Material 3 is an internal titanium housing. This is modelled as air since titanium is a non-magnetic material. Material 4 is the fluid chamber of the brake which includes both the MR fluid and the steel blades. A large atmospheric area is modelled around the brake to simulate its surroundings. As was mentioned in chapter 2 the brake actuator is approximately axi-symmetrical and therefore the model is 2D axi-symmetric. The axis of symmetry is shown in Figure 4-1.

Element

The finite element software Ansys [26] is used in the analysis. The PLANE13 elements were used to model the magnetic flux density. This element is defined by four nodes, see Figure 4-2, with up to four degrees of freedom per node. Possible degrees of freedom are magnetic vector potential in Z direction, temperature, displacement in X direction, displacement in Y direction and electric scalar potential.

Table 4-1. List of symbols.

Symbol	Description
B	Magnetic flux density
H	Magnetic field strength
J_s	Source current density
I	Current in coil
A	Coil Area
μ	Magnetic permeability

Table 4-1 shows the symbols used in the finite element study and a brief description for each one.

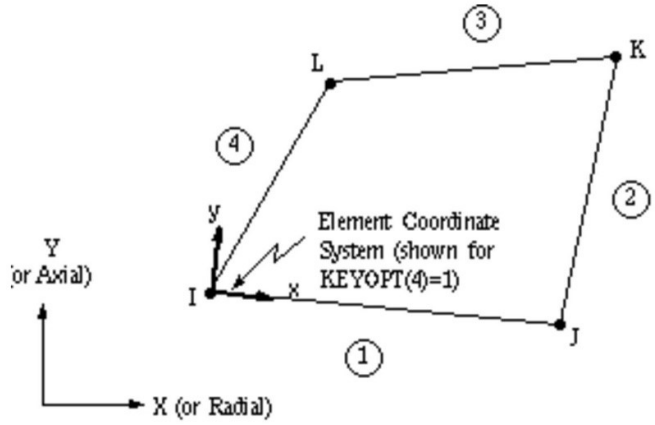

Figure 4-2. The PLANE13 2-D element in Ansys.

The element has nonlinear magnetic capability for modeling B-H curves. Each materials magnetic properties is implemented into the model with a table representing its B-H properties. The current in the model is static at 1.5 A and is input in the model in the form of source current density over the area of the coil:

$$J_s = \frac{n_{coil} I}{A} \qquad (11)$$

where n_{coil} is the number of windings in the coil, I is the current and A is the coil area. The solution output is sum of vector magnitudes of B.

Material Properties

The material properties [14] for the finite element model are acquired from non-linear B-H curves that express the magnetic permeability of the materials. Magnetic permeability describes a materials ability to support the formation of a magnetic field within itself. This results in a non-linear finite element analysis.

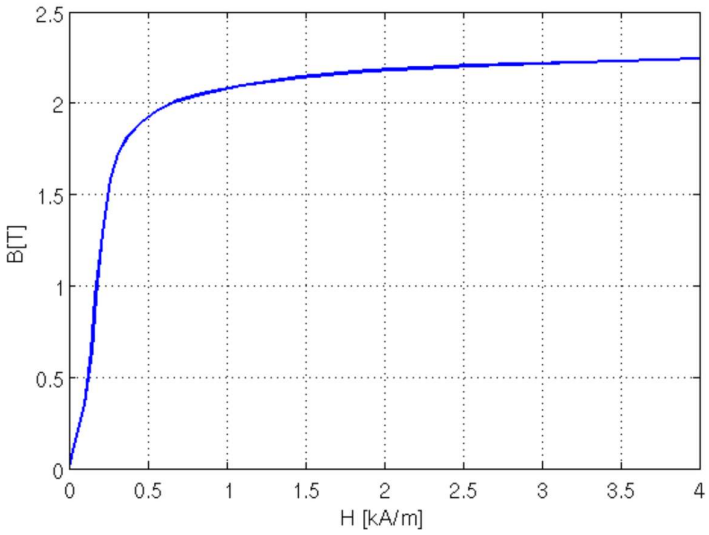

Figure 4-3. B-H curve for Cobalt-Iron alloy [27].

Figure 4-3 shows the B-H curve for the cobalt-iron alloy [27] with a magnetic saturation value around 2.35 T.

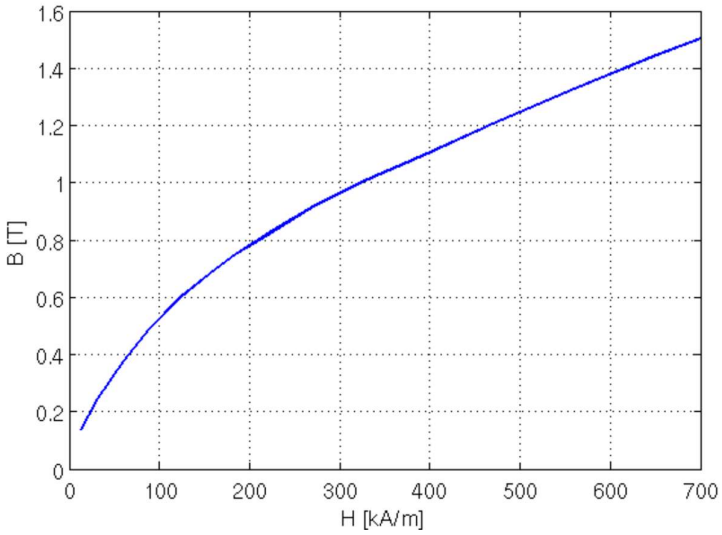

Figure 4-4. B-H curve for the reference MR fluid [14].

Figure 4-4 shows the B-H curve for the reference MR fluid. When compared to the cobalt-iron alloy the MR fluid has a more linear magnetic property when the applied magnetic field is small. As it increases a gradual magnetic saturation is observed, and the MR fluid's yield stress saturates.

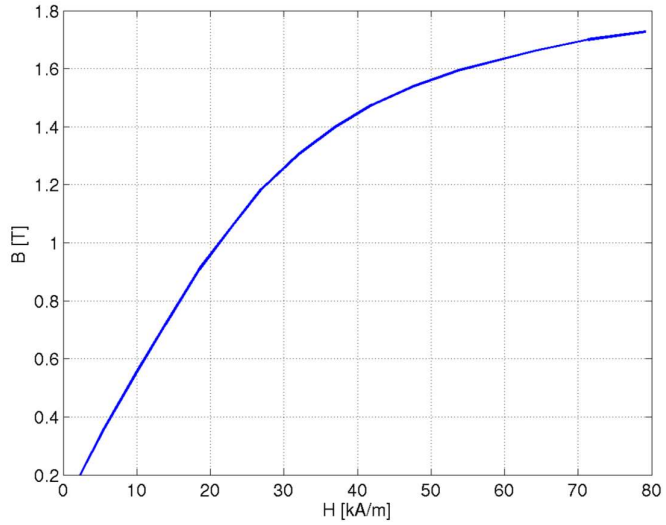

Figure 4-5. B-H curve for the steel blades in the fluid chamber [14].

Figure 4-5 shows the B-H curve for the steel blades. The steel blades have a noticeable lower saturation value than the cobalt-iron alloy and they reach the saturation at a much higher excitation. This shows that the cobalt-iron alloy is a better magnetic magnifier when compared to standard steel.

The magnetic behavior of the titanium internal housing as well as the atmosphere surrounding the MR rotary brake is described with a constant $\mu = 1.257\times10^{-6}\ {}^{H}/_{m}$.

The magnetic field produced by the coil is determined by the load applied to it as a current. As was mentioned in chapter 3 the current is kept at a constant value of 1.5 A. The magnetic field intensity then becomes

$$H = \frac{N \cdot I}{l} \qquad (12)$$

where the length of the coil, l, is 1.88 cm and the number of windings, N, varies from 300 to 400.

Model results

Figure 4-6 shows the flux lines in the model indicating how the magnetic field is conducted through the brake with minimum flux leakage. Figure 4-6. A finite element solution showing the flux lines in the model. flux lines for one solution.

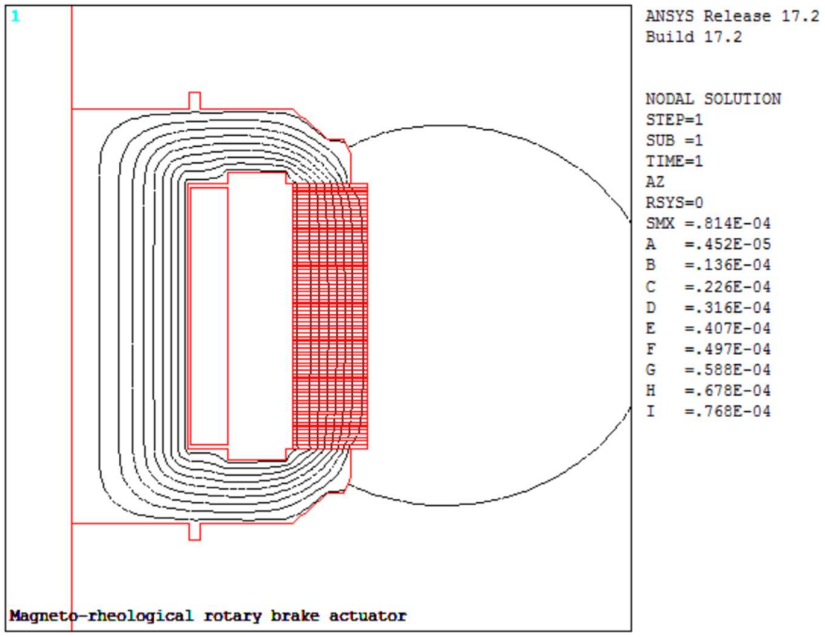

Figure 4-6. A finite element solution showing the flux lines in the model.

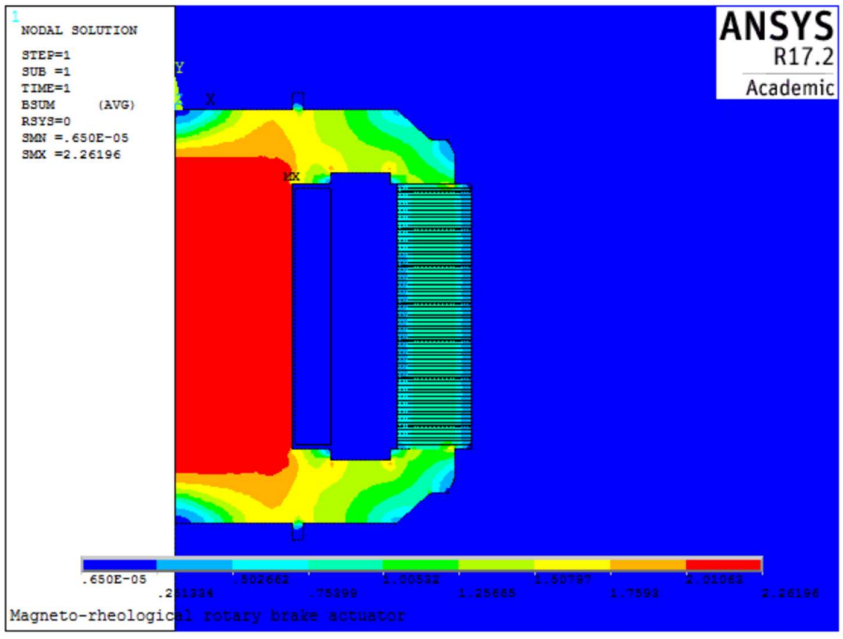

Figure 4-7. A finite element solution showing the MFD in the brake in Tesla.

Figure 4-7 shows the MFD in a scaled down version of the MR rotary brake. The core is at its saturation value of 2.26 T in accordance with the B-H curve for the core (Figure 4-3). The figure also shows that the magnetic field outside the brake is negligible proving that the magnetic circuit is well isolated. The MFD decreases in the core sides and reaches its lowest value of 0.25 T on the outskirts of the fluid chamber.

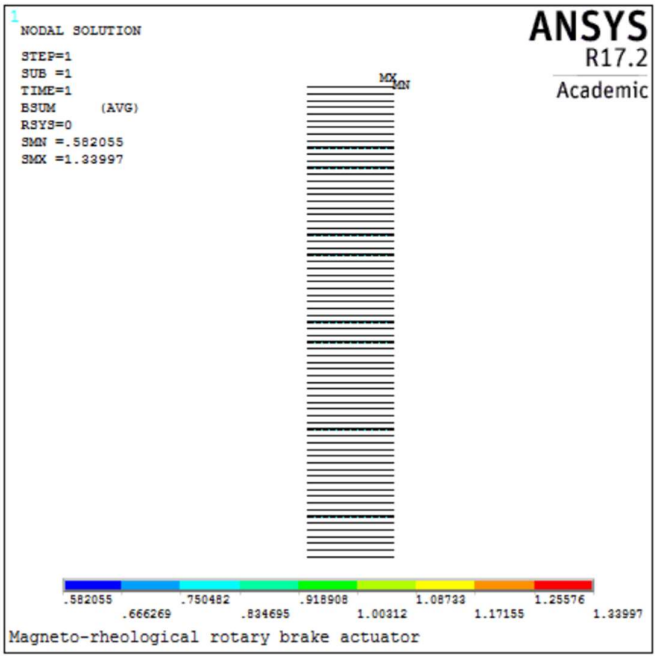

Figure 4-8. A finite element solution showing the MFD in the fluid.

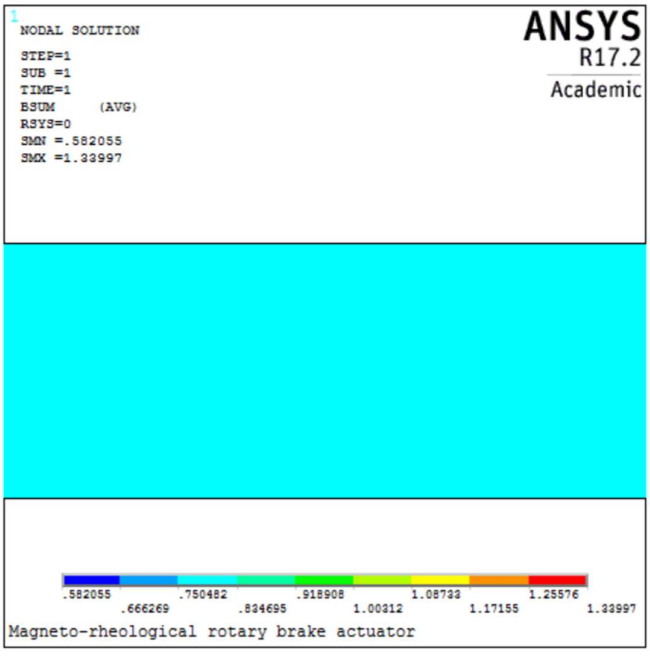

Figure 4-9. An enlarged view of finite element solution showing MFD in a fluid gap.

As was discussed in chapter 2 the fluid chamber consists of both the MR fluid and the steel blades and figure Figure 4-7 shows the MFD for the whole fluid chamber. Figure 4-8 shows the MFD in the MR fluid without the blades and as can be seen on the enlarged section in Figure 4-9 the average MFD in the fluid is close to 0.75 T. This is an example where the thickness of the fluid chamber is 3.5 mm and the radius of the core is 8.5 mm, resulting in a high MFD. A finite element solution is simulated for a number of parameters and a certain range for each. The results are used to calculate the braking torque in chapter 5 where for each design case the MFD in the fluid is used with Figure 2-6 and equation 7 to determine the yield stress of the MR fluid.

The finite element model simulates the magnetic flux density which is a crucial factor in calculating the braking torque in the rotary brake. It also provides a visual perspective and a better understanding of the effect different parameters have on the magnetic field, and therefore the braking torque. In the next chapter this will be inspected further.

5 Parameter analysis

The aim of the parameter analysis is to see how each parameter listed in Table 5-1 affects the braking torque and utilize that information to minimize the size of the MR rotary brake. While minimizing the size the braking torque needs to be within limits given in chapter 3.

Table 5-1. List of parameters tested.

Parameter	Description	Range tested
r_c [mm]	Radius of the core.	6 - 10
n_{coil}	Number of windings in the coil.	300 - 400
t_{fc} [mm]	Thickness of the fluid chamber.	3 - 7
r_o [mm]	Outer radius of the brake.	17 - 20
d [µm]	Gap between steel blades.	20 - 40

Changing the number of windings in the coil has an effect on the MFD and the torque output, but the range tested is narrow and has insignificant effect. All the following tests were done with 400 windings in the coil.

Figure 5-1 shows the effect increasing the core radius has on the braking torque output of the brake, and the black line indicates the proposed design criteria for minimum torque output. The graph indicates an almost linear relationship between the core radius and the braking torque.

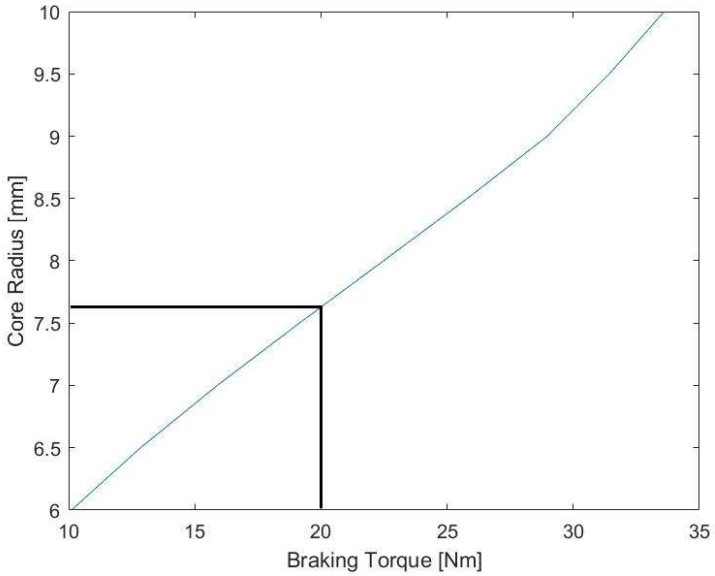

Figure 5-1. Core radius vs braking torque with fixed fluid chamber thickness of 3.5mm.

Table 5.2 shows the values for the core radius, magnetic flux density, outer radius and braking torque when fluid chamber thickness is fixed at 3.5 mm. The MFD and the torque increase with increased core radius and two values give braking torque over 20 Nm while outer radius is under 20 mm.

Table 5-2. Braking torque with increasing core radius.

r_c [mm]	MFD [T]	r_o [mm]	T [Nm]
6	0.46	17.17	10.11
6.5	0.52	17.67	12.85
7	0.58	18.17	15.89
7.5	0.64	18.67	19.14
8	0.69	19.17	22.47
8.5	0.75	19.67	25.80
9	0.80	20.17	28.97
9.5	0.84	20.67	31.43
10	0.85	21.17	33.60

Figure 5-2 shows the effect increasing the fluid chamber thickness has on the braking torque output. Increasing the thickness of the fluid chamber increases the braking torque overall, but unpredictably.

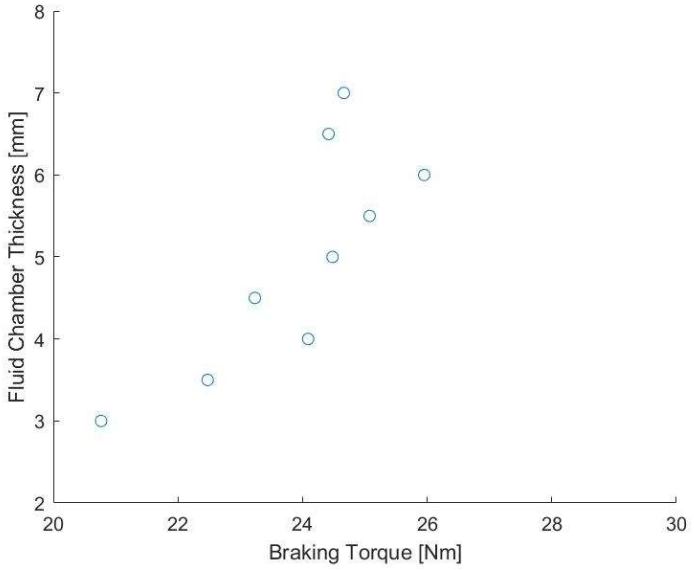

Figure 5-2. Fluid chamber thickness vs braking torque with fixed core radius of 8mm.

Table 5.3 shows the values for fluid chamber thickness, magnetic flux density, outer radius and braking torque when core radius is fixed at 8 mm. The MFD decreases with increased fluid chamber thickness while the braking torque increases overall. This is because the difference between r_i and r_o is greater with higher t_{fc} and that affects the braking torque more

than the MFD through τ_y, see equation 6. With low t_{fc} the radius of the core can be greater and 20 Nm torque can be achieved with outer radius under 20 mm.

Table 5-3. Braking torque with increasing fluid chamber thickness.

t_{fc} [mm]	MFD [T]	r_o [mm]	T [Nm]
3	0.77	18.67	20.77
3.5	0.69	19.17	22.48
4	0.64	19.67	24.09
4.5	0.55	20.17	23.23
5	0.52	20.67	24.48
5.5	0.49	21.17	25.08
6	0.46	21.67	25.95
6.5	0.42	22.17	24.41
7	0.39	22.67	24.66

Figure 5-3 shows outer radius vs. braking torque for different fluid chamber thickness. The black box represents the limits given in chapter 3.The relationship between r_c and the braking torque is almost linear as was seen in Figure 5-1, meaning the lower the t_{fc} value the higher r_c can be, increasing the torque. This figure shows that for the model to stay within the limits the t_{fc} value must be less than 5 mm. This can be observed further in table 5.4 where all the design cases are listed with increasing torque output.

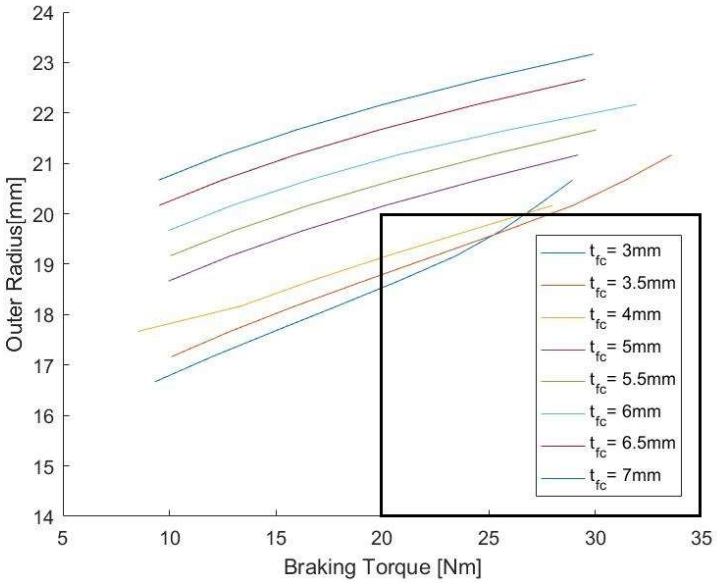

Figure 5-3. Outer radius vs braking torque where the values within the box are viable solutions considering the limits given.

Table 5-4. Tested parameters and values with increasing torque output.

r_c [mm]	t_{fc} [mm]	MFD [T]	r_o [mm]	T [Nm]
7.0	3.5	0.58	18.17	15.89
7.0	6.5	0.34	21.17	15.91
7.0	7.0	0.32	21.67	15.98
7.0	5.0	0.43	19.67	16.28
7.0	6.0	0.37	20.67	16.54
7.0	5.5	0.40	20.17	16.54
7.0	4.0	0.53	18.67	16.63
7.5	3.0	0.70	18.17	17.87
7.5	3.5	0.64	18.67	19.14
7.5	6.5	0.38	21.67	19.88
7.5	7.0	0.36	22.17	20.03
7.5	5.0	0.48	20.17	20.16
7.5	4.0	0.58	19.17	20.25
7.5	5.5	0.45	20.67	20.56
7.5	6.0	0.42	21.17	20.71
8.0	3.0	0.77	18.67	20.77
8.0	3.5	0.69	19.17	22.48
8.0	4.5	0.56	20.17	23.23
8.5	3.0	0.84	19.17	23.47
8.0	4.0	0.64	19.67	24.09
8.0	6.5	0.42	22.17	24.42
8.0	5.0	0.52	20.67	24.48
8.0	7.0	0.39	22.67	24.66
8.0	5.5	0.49	21.17	25.08
9.0	3.0	0.88	19.67	25.59
8.5	3.5	0.75	19.67	25.80
8.0	6.0	0.46	21.67	25.95
9.5	3.0	0.90	20.17	27.30
8.5	4.0	0.69	20.17	28.00
10	3.0	0.91	20.67	28.94
9.0	3.5	0.80	20.17	28.97
8.5	5.0	0.57	21.17	29.20
8.5	6.5	0.45	22.67	29.54
8.5	7.0	0.43	23.17	29.91
8.5	5.5	0.53	21.67	30.06
9.5	3.5	0.84	20.67	31.43
8.5	6.0	0.51	22.17	31.92
10	3.5	0.85	21.17	33.60

Decreasing the gap between the steel blades in the fluid chamber increases the braking torque by some degree without effecting the outer radius. This can be utilized but with limitations since it increases the off-state braking torque and can make the joint stiff. Table 5.5 shows the result of changing the gap between blades from 20 µm up to 40 µm in a brake with core radius of 8.5 mm and fluid chamber thickness of 3.5 mm. For these calculations in order to increase the gap size the thickness of the steel blades is decreased.

Table 5-5. Gap between blades, braking torque and off-state torque.

d [µm]	T [Nm]	$T_{off\text{-}state}$ [Nm]
20	26.46	1.95
25	26.15	1.88
30	25.95	1.83
35	25.80	1.80
40	25.68	1.78

Increasing the number of blades, n, can be utilized to increase the braking torque. This can affect the width of the brake or decrease the gap size, and is not taken into consideration in this thesis.

Table 5-6. Difference between compact design and reference design.

Parameter	Reference design	Compact design	Decrease [%]
r_c [mm]	10.7	8.5	20.6
n_{coils}	310	400	-29.0
t_{fc} [mm]	6.5	3.5	46.2
r_o [mm]	24.27	19.67	19.0
n	71	71	0
d [µm]	35	35	0
T [Nm]	61	25.8	57.7

Table 5-6 shows the difference between the compact design and the reference design. While the compact design is within given size and torque limits, 57.7% torque reduction has occurred while the size has only been reduced by 19%. It should be taken into consideration that the reference design is optimized for maximum torque output while the compact design is not.

While the required torque output can be reached within the size limits discussed it should be noted that increasing the outer radius by a small amount, the torque output can be increased significantly. For an example a brake with outer radius of 19.67 mm has an output torque of 25.8 Nm while a brake with outer radius of 21.17 mm has an output torque of 33.6 Nm. That is an 8% increase in diameter resulting in a 30% increase in torque output. This can be further observed in Table 5-4.

6 Conclusion

In this thesis an optimized model of an MR rotary brake used in a prosthetic knee was scaled down to test its effectiveness in the more compact environment of a foot prosthesis. This was achieved by limiting the radius of the core, the thickness of the fluid chamber and the number of windings in the coil. FEM analysis was then used to simulate the magnetic flux density in the brake and evaluate the effect that chosen parameters had on its size and the torque output.

Parameter analysis indicates that increasing the core radius while minimizing the thickness of the fluid chamber is the most effective method to maintain torque output above 20 Nm while keeping the outer radius of the brake below 20 mm. The limiting factor for the torque output is how small the steel blades in the fluid chamber can be manufactured.

This thesis indicates that a compact version of the MR rotary brake can be utilized in a prosthetic foot. However it is clear that decreasing the size of the brake has significant effect on the torque output. This can be attributed by some extend to reference design being optimized where the compact design is not. It should also be noted that by increasing the size of the brake by a small amount the torque can be increased significantly. For further studies the compact design could be optimized with regard to torque output and size. The effect of increasing the width of the brake was shortly discussed but could be studied further. The MR fluid used for this study was originally chosen for the reference design, a prosthetic knee, where low off-state torque is required. This is not as crucial in a prosthetic foot. Different MR fluids that result in higher on- and off-state torque output could be studied for this design.

References

1. Hansen, A.H., et al., *The human ankle during walking: implications for design of biomimetic ankle prostheses.* Journal of Biomechanics, 2004. **37**(10): p. 1467-1474.
2. Gudmundsson, K.H., F. Jonsdottir, and F. Thorsteinsson, *A geometrical optimization of a magneto-rheological rotary brake in a prosthetic knee.* Smart Materials and Structures, 2010. **19**(3): p. 035023.
3. Verma, S., N. Kumar, and A. Kumar, *Design analysis of variable damping mechanism using magnetorheological fluids for adaptive prosthetic foot.* 2013.
4. Koniuk, W., *Self-adjusting prosthetic ankle apparatus*. 2002, Google Patents.
5. Guðmundsson, Í., *A feasibility study of magnetorheological elastomers for a potential application in prosthetic devices. 2011*, Masters Thesis, University of Iceland.
6. *BIONX*. 2017 02.05.2017]; Available from: http://www.bionxmed.com/.
7. *Össur*. 2017; Available from: http://www.ossur.is/.
8. Jolly, M.R., J.W. Bender, and J.D. Carlson, *Properties and Applications of Commercial Magnetorheological Fluids.* Journal of Intelligent Material Systems and Structures, 1999. **10**(1): p. 5-13.
9. Jacob, R., *Magnetic fluid torque and force transmitting device*. 1951, Google Patents.
10. Carlson, J.D., D.M. Catanzarite, and K.A. St. Clair, *COMMERCIAL MAGNETO-RHEOLOGICAL FLUID DEVICES.* International Journal of Modern Physics B, 1996. **10**(23n24): p. 2857-2865.
11. Carlson, J.D. and M.R. Jolly, *MR fluid, foam and elastomer devices.* Mechatronics, 2000. **10**(4–5): p. 555-569.
12. Note, L.C.E., *Designing with MR Fluids*, T.L.R. Center, Editor. 1999, Lord Corporation: Cary, NC.
13. Hsu, H., et al., *Magnetorheological fluid compositions and prosthetic knees utilizing same*. 2006, Google Patents.
14. Jonsdottir, F., et al., *Bidisperse Perfluorinated Polyether (PFPE)-Based Magneto-Rheological Fluids in a Prosthetic Knee.* 2009(48968): p. 15-22.
15. Phillips, R.W., *Engineering applications of fluids with a variable yield stress*. 1969.
16. Sadok, S., et al., *An innovative magnetorheological damper for automotive suspension: from design to experimental characterization.* Smart Materials and Structures, 2005. **14**(4): p. 811.
17. Poynor, J., *Innovative Designs for Magneto-Rheological Dampers*, in *Mechanical Engineering*. 2001, Virginia Polytechnic Institute and State University: Virginia.
18. Carlson, J.D., et al., *Controllable vibration apparatus*. 1999, Google Patents.
19. Herr, H. and A. Wilkenfeld, *User-adaptive control of a magnetorheological prosthetic knee.* Industrial Robot: An International Journal, 2003. **30**(1): p. 42-55.
20. Deffenbaugh, B.W., et al., *Electronically controlled prosthetic knee*. 2004, Google Patents.
21. Jonsdottir, F., et al., *Influence of Parameter Variations on the Braking Torque of a Magnetorheological Prosthetic Knee.* Journal of Intelligent Material Systems and Structures, 2009. **20**(6): p. 659-667.

22. Guðmundsson, K.H., *Design of a magnetorheological fluid for an MR prosthetic knee actuator with an optimal geometry.* 2011, Ph.D. Thesis, University of Iceland.
23. Spencer Jr, B., et al., *Phenomenological model for magnetorheological dampers.* Journal of engineering mechanics, 1997. **123**(3): p. 230-238.
24. Au, S.K., J. Weber, and H. Herr. *Biomechanical design of a powered ankle-foot prosthesis*. in *Rehabilitation Robotics, 2007. ICORR 2007. IEEE 10th International Conference on*. 2007. IEEE.
25. Thorarinsson, E.T., F. Jonsdottir, and H. Palsson, *Finite element analysis of a magnetorheological prosthetic knee.* Development Process: From Idea to the World's First Bionic Prosthetic Foot, 2006.
26. ANSYS. *ANSYS*. 2017; Available from: http://www.ansys.com.
27. *Vacuumschmelze*. [cited 2017 01.05.2017]; Available from: http://www.vacuumschmelze.de/.